

Improving Histogram-based Reversible Information Hiding by an Optimal Weight-based Prediction Scheme

Shih-Lun Lin

Department of Computer Science and Information Engineering
National University of Kaohsiung
700, Kaohsiung University Rd., Nanzih District, Kaohsiung, 811, Taiwan
P76004334@mail.ncku.edu.tw

Chien-Feng Huang

Department of Computer Science and Information Engineering
National University of Kaohsiung
700, Kaohsiung University Rd., Nanzih District, Kaohsiung, 811, Taiwan
Tel: +886-7-591-9798
Fax: +886-7-591-9514
cfhuang15@nuk.edu.tw

Meng-Huan Liou

Department of Computer Science and Information Engineering
National University of Kaohsiung
700, Kaohsiung University Rd., Nanzih District, Kaohsiung, 811, Taiwan
A0975554@mail.nuk.edu.tw

Chien-Yuan Chen

Department of Computer Science and Information Engineering
National University of Kaohsiung
700, Kaohsiung University Rd., Nanzih District, Kaohsiung, 811, Taiwan
Tel: +886-7-591-9504
cychen07@nuk.edu.tw

Received September 2011; revised November 2012

ABSTRACT. *Information hiding has been an important research area for copyright protection in modern multimedia technologies. In this paper, a weight-based prediction scheme is presented to enhance the performance of several reversible histogram-based data hiding approaches. By computing the solution of the least-squares problem, we obtain the optimal set of weights for the neighboring pixels to improve the prediction accuracy of the target pixel across the whole image. The heights of the peak points in the histogram can then be raised to increase the embedding capacity. Experiments of our proposed algorithm have been conducted over several well-known test images. We will show that our proposed method significantly improves the embedding capacity upon several methods and still maintains the quality of stego-images.*

Keywords: Histogram-based information hiding, weight-based prediction, optimal least-squares solutions, embedding capacity.

1. Introduction. Along with the advancement of multimedia technologies in the past decades, storage of data by digital products or transmission of data over the Internet, in the form of texts, images or videos, have brought about significant progress for modern information technology. Nonetheless, the increasingly powerful software has also made it easy to gain unrestricted access to the data in the storage media for further modifying its content. As a result, data and copyright protection have been important subjects in research and applications nowadays. On the other hand, during the process of data transmission, it often occurs that confidential information needs to be encrypted in order to avoid interception by attackers in communication networks. To solve these problems, several information hiding methods have been proposed and studied for data protection and secret information embedding, but these traditional data hiding techniques often bring about permanent damage to the content of the host media, which is not acceptable in some applications [1].

More recently, a significant amount of research to improve the effectiveness on information hiding has been conducted. These developed techniques typically intend to strengthen their effectiveness by increasing the amount of data being embedded while maintaining good quality of reconstruction for the host media. According to Yang and Tsai [2], the methodologies developed along this line of research for reversible data hiding can be classified into two main areas: (1) the difference-expansion-based approaches [3-11], and (2) the histogram-based data hiding approaches [12-18].

Difference expansion is a popular technique for information embedding. Earlier work developed by Tian [7] along this line of research was a high-capacity and low-distortion reversible data hiding scheme based on difference expansion transform on pairs of pixels. His algorithm attempted to embed bits of data into the difference of the pixels of pairs that do not cause an overrow or underrow. In addition, a location map for which pairs being embedded data is compressed and included in the payload. In order to improve Tians method, Chang and Lu [8] then proposed to determine the degree of the difference expansion for data embedding by the correlation between target pixels and their surrounding pixels. They showed that their correlation-based method can improve both the embedding ability and the computation efficiency. On the other hand, Alattar [9] extended Tians method by using a difference expansion of vectors, instead of pairs, to further increase the hiding ability. However, these aforementioned methods have limited potential in practical applications because location maps and other extra information are needed to restore the original cover image, and they usually lack sufficient robustness [1].

In 2006, Ni *et al.* [12] presented a histogram-based data hiding technique. They proposed to construct the histogram by pixel values and embed the information using the vacancy between peak points and zero points. Ni *et al.*'s method guarantees that the change of the intensity levels of pixels in the stego-images is no more than 1. As a result, the peak signal-to-noise ratio (PSNR) value of the stego-image is at least 48 dB. Afterwards, Hong *et al.* [13], Yang *et al.* [2], and Lin *et al.* [18] presented a set of prediction schemes to increase the embedding capacity by elevating the peak value of the histogram. Overall, the histogram-based methods utilize the distribution characteristics of the histogram to achieve the task of reversible data hiding. Because of the robustness and low computational complexity, this type of data hiding methods has received increasing interests [1].

In the three aforementioned prediction-based methods [1-2, 18], the neighboring pixels are usually used to predict the intensity level of a target pixel. These methods employ several heuristics to reduce the prediction errors locally without taking into account how to minimize the errors globally over the whole image. Motivated by this observation, in this paper we propose a new approach, called the weighted prediction, to compute the

optimal weights of the neighboring pixels for the prediction of target pixels over the whole image. We will show that this new weighted prediction method is able to improve the three prediction-based methods by raising the embedding capacity effectively and still yield satisfactory image quality.

The organization of this paper is as follows. In Section 2, we discuss the relevant research work of the histogram-based data hiding approaches using prediction schemes. Section 3 describes our proposed method. Section 4 then demonstrates the experimental results, and conclusions are given in Sections 5.

2. Related Work. Ni *et al.* [12] first proposed a reversible data hiding method that constructs the histogram for intensity levels of pixels of a host image to embed secret information. The histogram is then used to identify pairs of zero and peak points, which represent the values that none and most pixels assume in the cover image, respectively. The space between a pair of peak and zero points can be shifted in order to generate free space for embedding of the secret information.

Hong *et al.* [13] proposed a different scheme to construct the histogram using a difference image generated by the median edge detection predictor [19, 21]. The goal of this treatment was to generate a more centralized histogram and raise the height of the peak points to improve the embedding capacity upon the histogram-based method Ni *et al.* [12] proposed.

Yang *et al.* [2] proposed a new scheme using column-based interleaving predictions to enhance the performance of the histogram-based approach. In this scheme, the odd-column pixels are predicted by pixels in even columns; then the even-column pixels are predicted by pixels in odd columns, or vice versa. Yang *et al.* [2] also studied a chessboard prediction method, which is an extension of the original interleaving prediction scheme. Because the prediction errors can be reduced significantly, the heights of the peak points can be raised further to increase the embedding capacity. In addition to the increase in embedding capacity, Yang *et al.* [2] showed that their histogram-based approach can also yield a better image quality, compared to several other histogram-based approaches.

Lin *et al.* [18] later proposed a 3-by-3 box filter scheme to improve the embedding capacity for complex images upon the chessboard-based method. In smooth images, the differences among the intensity levels of neighboring pixels may be small; thus averaging the intensity levels of the four adjacent pixels by Yang *et al.*'s method would predict the target pixel well. However, in complex images, more neighboring pixels may be required for better prediction. Lin *et al.* [18] thus proposed to increase the number of the reference pixels to eight by using the 33 box filter, and the prediction of the target pixel is then the average of the eight surrounding pixels. Lin *et al.* [18] also proposed to improve Yang *et al.*'s approach [2] by replacing the proposed floor function with the truncation function. Since the prediction-error histogram using the truncation function has higher tendency to center around zero than the floor function does, the embedding capacity can be further increased.

Since Lin *et al.*'s method in [18] was written in Chinese and we intend to improve their method, in the remaining of this subsection, we provide the description for the steps of this algorithm.

2.1. Lin *et al.*'s algorithm. The order of the pixels to be predicted in this scheme is divided into 4 stages, as show in Fig. 1, with the coordinate of each stage's starting pixel, (T_x, T_y) , being $(0, 0)$, $(0, 1)$, $(1, 0)$ and $(1, 1)$, respectively.

In this study, all original images are composed of 512×512 pixels. Let $H_{i,j}$ with $\{i, j \in 0 \sim 511\}$ denote the intensity level of the pixel at column i and row j in the original

I	II	I	II
III	IV	III	IV
I	II	I	II
III	IV	III	IV

FIGURE 1. Numerical orders of pixels to be predicted

image. Let $D_{i,j}$ denote the predictive error of $H_{i,j}$. Also let $S_{i,j}$ denote the set of all the closest pixels surrounding $H_{i,j}$; i.e.,

$$S_{i,j} = \{H_{x,y} \mid x, y \in 0 \sim 511, 0 < (i-x)^2 + (j-y)^2 \leq 2\}. \quad (2.1)$$

Let $D_{i,j}$ denote the predictive error of $H_{i,j}$, calculated as follows:

$$D_{i,j} = \text{Int}\left(H_{i,j} - \frac{\sum_{h \in S_{i,j}} h}{|S_{i,j}|}\right). \quad (2.2)$$

Note that function Int in Eq. 2.2 is used to truncate the fractional portion of the prediction errors. However, before using function Int , we will record the sign of the value of the difference for the recovering step, which is described in the next subsection (i.e., Step 5 in Section 2.1.1).

$$s = \text{sign}\left(H_{i,j} - \left(\frac{\sum_{h \in S_{i,j}} h}{|S_{i,j}|}\right)\right), \quad (2.3)$$

$$\text{sign}(x) = \begin{cases} 1, & x > 0 \\ 0, & x = 0. \\ -1, & x < 0 \end{cases} \quad (2.4)$$

2.1.1. Hiding phase.

Input: original image H and secret information I .

Step 1. Use Eqs. 2.1 and 2.2 to generate predictive error, $D_{i,j}$'s, for (T_x, T_y) of the first stage.

Step 2. Create histogram $HS(x)$ with $\{x \in [-255, 255]\}$ from all predictive errors $D_{i,j}$'s and select two pairs of peak and zero points, $(P_{1,1}, Z_{1,1})$ and $(P_{1,2}, Z_{1,2})$,

Step 3. Shift histogram as follows:

$$D'_{i,j} = \begin{cases} D_{i,j} - 1, & Z_{1,1} < D_{i,j} \leq P_{1,1} - 1; \\ D_{i,j} + 1, & P_{1,2} + 1 \leq D_{i,j} < Z_{1,2}. \end{cases} \quad (2.5)$$

Step 4. Embed a secret bit if the predictive error $D'_{i,j}$ is equal to $P_{1,1}$ or $P_{1,2}$ as follows:

(a) If the to-be-embedded bit is 0, $D'_{i,j}$ is set to $D_{i,j}$.

(b) If the to-be-embedded bit is 1, $D'_{i,j}$ is set according to the following equation:

$$D'_{i,j} = \begin{cases} D_{i,j} - 1, & D_{i,j} = P_{1,1}; \\ D_{i,j} + 1, & D_{i,j} = P_{1,2}. \end{cases} \quad (2.6)$$

Step 5. Convert the predictive errors with the inserted secret information to pixel values, where the conversion formula is as follows:

$$H'_{i,j} = \begin{cases} \text{Int}(D'_{i,j} + \frac{\sum_{h \in S_{i,j}} h}{|S_{i,j}|}), & \text{if } s \leq 0; \\ \text{Int}(D'_{i,j} + \frac{\sum_{h \in S_{i,j}} h}{|S_{i,j}|}) + 1, & \text{otherwise.} \end{cases} \quad (2.7)$$

Step 6. Repeat Steps 1-5 for the corresponding starting point (T_x, T_y) of all the other stages to insert the remaining secret information.

Step 7. Output stego-image H' and four pairs of peak and zero points

2.1.2. Extracting phase.

Input: stego-image H' , four pairs of peak and zero points.

Step 1. Use Eqs. 2.1 and 2.2 to generate prediction errors in the reverse order of the hiding phase. Use fourth pair of peak and zero points and Eq. 2.8 to extract information I_4 , and use Eq. 2.9 to recover the predictive error values. Let $I_{4,n}$ is the n -th bit in I_4 .

$$I_{4,n} = \begin{cases} 0, & \text{if } D_{i,j} = P_{4,1} \text{ or } D_{i,j} = P_{4,2}, \\ 1, & \text{if } D_{i,j} = P_{4,1} - 1 \text{ or } D_{i,j} = P_{4,2} + 1. \end{cases} \quad (2.8)$$

$$D'_{i,j} = \begin{cases} D_{i,j} + 1, & Z_{4,1} < D_{i,j} \leq P_{4,1} - 1; \\ D_{i,j} - 1, & P_{4,2} + 1 \leq D_{i,j} < Z_{4,2}. \end{cases} \quad (2.9)$$

Step 2. Use Eq. 2.7 to reconstruct the pixel values for the fourth stage.

Step 3. For all the remaining stages, repeat steps 1-3 to extract the inserted secret information I_3, I_2 and I_1 and then the corresponding pixels will be recovered to the original values.

Step 4. Output original image H and secret information $I = I_1 || I_2 || I_3 || I_4$.

3. Our method. The goal of prediction is to introduce a centralized histogram constructed by the differences between the actual and predicted values of pixels the more centralized the histogram is, the more embedding capacity the image delivers. In this study, we propose to improve the aforementioned prediction-based data hiding methods by computing the optimal weights of the neighboring pixels for the prediction of the target pixel. In contrast to the methods proposed by Hong *et al.* [13], Yang *et al.* [2], Lin *et al.* [18] that did not consider minimizing the overall prediction errors over all the pixels simultaneously, we hereby propose to compute the optimal weights of the neighboring pixels in terms of the least-squared prediction errors across the whole image.

Consider the following example:

In Lin *et al.* [18], the prediction scheme used the average of the intensity levels of the eight surrounding pixels as the predicted intensity level of the target pixel (the outermost pixels are not being predicted because the number of the neighboring pixels is less than 8). Now we generate a $n \times 8$ matrix A with each row representing the eight surrounding pixels used to predict the target, and a $n \times 1$ column vector B with each element representing the target pixel to be predicted. Then solving the equation,

$$Ax = B, \quad (3.1)$$

the least-squared solution x can be regarded as the weighting vector used for the prediction of the pixels in B . For instance, the example in Fig. 2 can be expressed as follows:

20	29	43	71	120	202
22	32	53	90	152	196
24	40	68	114	147	175
30	51	85	110	132	156
38	64	83	99	117	139
48	62	74	88	104	122

FIGURE 2. Example image

$$\begin{bmatrix} 20 & 29 & 43 & 22 & 53 & 24 & 40 & 68 \\ 29 & 43 & 71 & 32 & 90 & 40 & 68 & 114 \\ 43 & 71 & 120 & 53 & 152 & 68 & 114 & 147 \\ \vdots & \vdots \end{bmatrix} x = \begin{bmatrix} 32 \\ 53 \\ 90 \\ \vdots \end{bmatrix} \quad (3.2)$$

where $x = [x_1 \ x_2 \ x_3 \ x_4 \ x_5 \ x_6 \ x_7 \ x_8]^T$.

The optimal solution x then guarantees all prediction errors to be zero. Furthermore, for Fig. 2, all the 16 to-be-predicted pixels are embeddable. Thus the embedding capacity is 16 bits, yet the capacity in same figure is only 8 bits by the 3-by-3 box filter method (see Fig. 3 below). As a result, the improvement of the embedding capacity is significant by our proposed method.

20	29	43	71	120	202
22	-5	-7	-6	12	196
24	-5	-3	9	6	175
30	-3	6	4	0	156
38	5	3	0	-2	139
48	62	74	88	104	122

FIGURE 3. Predicted example image

More specifically, suppose the original images are composed of 512×512 pixels. Let $S_{i,j}$ with $\{i, j \in 0 \sim 511\}$ denote the intensity level of the pixel at column i and row j in the original image. Since the outermost pixels are not used for prediction, let $R_{i,j}$ denote the set of all the closest pixels around $S_{i,j}$ that are used for prediction; i.e.,

$$R_{i,j} = \{S_{i,j} | x, y \in 1 \sim 510, 0 < (i - x)^2 + (j - y)^2 \leq 2\}. \quad (3.3)$$

Use all the $R_{i,j}$'s and target pixels $S_{i,j}$'s, one can generate an $n \times 8$ matrix A and an $n \times 1$ matrix B , respectively. Let x denote the vector of weights to be used for prediction. Assuming the prediction error is zero for each pixel, then the following equation holds:

$$Ax = B, \quad (3.4)$$

In general, one cannot expect to find a vector x for which Ax equals B . Instead, in this overdetermined system one can look for a vector x such that Ax is closest to B .

Let $r(x)$ denote the residual:

$$r(x) = B - Ax. \quad (3.5)$$

A vector \hat{x} with the minimum $r(x)$ is said to be optimal to the system $Ax = B$. Then \hat{x} will be the least squares solution to the system $Ax = B$ if and only if

$$r(\hat{x}) \in N(A^T) \quad (\text{Theorem 5.3.1[22]})$$

or, equivalently,

$$0 = A^T r(\hat{x}) = A^T \times (B - Ax). \quad (3.6)$$

To solve the least squares problem $Ax = B$, one must solve the normal equations:

$$A^T A \hat{x} = A^T B. \quad (3.7)$$

Then the unique solution of the normal equations is:

$$\hat{x} = (A^T A)^{-1} A^T B. \quad (3.8)$$

The solution \hat{x} can then serve as the optimal weights for computing the prediction of the intensity level for each pixel $N_{i,j}$ by the following formula:

$$N_{i,j} = R_{i,j} \hat{x}. \quad (3.9)$$

Therefore, the prediction error $D_{i,j}$ of $S_{i,j}$ is:

$$D_{i,j} = \text{Int}(S_{i,j} - \frac{\sum_{h \in N_{i,j}} h}{|N_{i,j}|}). \quad (3.10)$$

Note that function Int in Eq. 3.10 is used to truncate the fractional portion of the prediction errors.

To further understand the characteristics of this optimal weight-based scheme, we provide the following theorem. Let $A_{m \times n}$ be an $m \times n$ matrix, $x_{n \times 1}$ be an $n \times 1$ matrix, and $B_{m \times 1}$ be an $m \times 1$ matrix. We then define the rows of $A_{m \times n}$ as the matrices A_1, A_2, \dots, A_m . We further let $A_{r \times n}$ be the submatrix of $A_{m \times n}$ and $B_{r \times 1}$ be the submatrix of $B_{m \times 1}$ for $r \leq m$, respectively.

Theorem 3.1. *Let \hat{x} be the least-square solution to $A_{m \times n} x_{n \times 1} = B_{m \times 1}$ and \hat{x}' be the least-square solution to $A_{r \times n} x_{n \times 1} = B_{r \times 1}$, where $r \leq m$. We then have*

$$\|A_{r \times n} \hat{x}' - B_{r \times 1}\| \leq \|A_{m \times n} \hat{x} - B_{m \times 1}\|.$$

Proof. We assume that $\|A_{r \times n} \hat{x}' - B_{r \times 1}\| > \|A_{m \times n} \hat{x} - B_{m \times 1}\|$.

We then have

$$\frac{\sqrt{(A_1\hat{x}' - b_1)^2 + (A_2\hat{x}' - b_2)^2 + \cdots + (A_r\hat{x}' - b_r)^2}}{\sqrt{(A_1\hat{x} - b_1)^2 + (A_2\hat{x} - b_2)^2 + \cdots + (A_r\hat{x} - b_r)^2 + \cdots + (A_m\hat{x} - b_m)^2}} >$$

where $B_{r \times 1} = \begin{bmatrix} b_1 \\ b_2 \\ \vdots \\ b_r \end{bmatrix}$ and $B_{m \times 1} = \begin{bmatrix} b_1 \\ b_2 \\ \vdots \\ b_m \end{bmatrix}$.

Because $(A_{r+1}\hat{x} - b_{r+1})^2 + \cdots + (A_m\hat{x} - b_m)^2 \geq 0$, we get

$$\frac{\sqrt{(A_1\hat{x}' - b_1)^2 + (A_2\hat{x}' - b_2)^2 + \cdots + (A_r\hat{x}' - b_r)^2}}{\sqrt{(A_1\hat{x} - b_1)^2 + (A_2\hat{x} - b_2)^2 + \cdots + (A_r\hat{x} - b_r)^2}} >$$

But, we know that \hat{x}' is the least-square solution to $A_{r \times n}x_{n \times 1} = B_{r \times 1}$. This implies that

$$\frac{\sqrt{(A_1\hat{x}' - b_1)^2 + (A_2\hat{x}' - b_2)^2 + \cdots + (A_r\hat{x}' - b_r)^2}}{\sqrt{(A_1\hat{x} - b_1)^2 + (A_2\hat{x} - b_2)^2 + \cdots + (A_r\hat{x} - b_r)^2}} \leq$$

That contradicts our assumption. We thus prove that $\|A_{r \times n}\hat{x}' - B_{r \times 1}\| \leq \|A_{m \times n}\hat{x} - B_{m \times 1}\|$ for $r \leq m$.

This theorem indicates that the least-square error increases as the size of the image increases.

In the following subsections, we describe the embedding and extracting phases of our algorithm. Let I denote the secret information to-be embedded and I_n denote the n -th bit of I .

□

3.1. Embedding Phase.

Input: original image S and secret information I . Output: stego-image S' , four sets of weights W_1 to W_4 , four pairs of peak and zero points: $(P_{1,1}, Z_{1,1})$, $(P_{1,2}, Z_{1,2})$, $(P_{2,1}, Z_{2,1})$, $(P_{2,2}, Z_{2,2})$, $(P_{3,1}, Z_{3,1})$, $(P_{3,2}, Z_{3,2})$, $(P_{4,1}, Z_{4,1})$ and $(P_{4,2}, Z_{4,2})$.

Step 1. Use Eq. 3.2 to Eq. 3.10 to calculate the optimal set of weight W_1 and generate predictive errors, $D_{i,j}$'s, for (T_x, T_y) of the first stage.

Step 2. Create histogram $HS(x)$ with $\{x \in [-255, 255]\}$ from all predictive errors $D_{i,j}$'s.

Step 3. Identify two pairs of peak and zero points, $(P_{1,1}, Z_{1,1})$ and $(P_{1,2}, Z_{1,2})$, as follows:

- (a) Select two highest peak points, $P_{1,1}$ and $P_{1,2}$, from $HS(x)$, where $P_{1,2} < P_{1,1}$.
- (b) Select a zero point $Z_{1,1}$ from $HS(x)$ with $\{x \in [-255, P_{1,1} - 1]\}$; select a zero point $Z_{1,2}$ from $HS(x)$ with $\{x \in [P_{1,2} + 1, 255]\}$.

Step 4. Shift the histogram as follows:

$$D'_{i,j} = \begin{cases} D_{i,j} - 1, & Z_{1,1} < D_{i,j} \leq P_{1,1} - 1; \\ D_{i,j} + 1, & P_{1,2} + 1 \leq D_{i,j} < Z_{1,2}. \end{cases} \quad (3.11)$$

Step 5. Embed a secret bit if the predictive error $D'_{i,j}$ is equal to $P_{1,1}$ or $P_{1,2}$ as follows:

- (a) If the to-be-embedded bit is 0, $D'_{i,j}$ is set to $D_{i,j}$.
- (b) If the to-be-embedded bit is 1, $D'_{i,j}$ is set according to the following equation:

$$D'_{i,j} = \begin{cases} D_{i,j} - 1, & D_{i,j} = P_{1,1}; \\ D_{i,j} + 1, & D_{i,j} = P_{1,2}. \end{cases} \quad (3.12)$$

Step 6. Convert the predictive errors with the inserted secret information to pixel values using the conversion equations below:

$$S'_{i,j} = \begin{cases} \text{Int}(D'_{i,j} + \frac{\sum_{h \in S_{i,j}} h}{|S_{i,j}|}), & \text{if } D'_{i,j} \leq 0 \text{ or } D'_{i,j} \text{ is integer;} \\ \text{Int}(D'_{i,j} + \frac{\sum_{h \in S_{i,j}} h}{|S_{i,j}|}) + 1, & \text{otherwise.} \end{cases} \quad (3.13)$$

Step 7. Repeat Steps 1-7 for the corresponding starting point (T_x, T_y) of all the other stages to insert the remaining secret information.

Step 8. Output stego-image S' , four sets of weight W_1 to W_4 , and four pairs of peak and zero points $(P_{1,1}, Z_{1,1})$, $(P_{1,2}, Z_{1,2})$, $(P_{2,1}, Z_{2,1})$, $(P_{2,2}, Z_{2,2})$, $(P_{3,1}, Z_{3,1})$, $(P_{3,2}, Z_{3,2})$, $(P_{4,1}, Z_{4,1})$ and $(P_{4,2}, Z_{4,2})$.

3.2. Extracting Phase.

Input: stego-image S' , four sets of weight W_1 to W_4 , four pairs of peak and zero points: $(P_{1,1}, Z_{1,1})$, $(P_{1,2}, Z_{1,2})$, $(P_{2,1}, Z_{2,1})$, $(P_{2,2}, Z_{2,2})$, $(P_{3,1}, Z_{3,1})$, $(P_{3,2}, Z_{3,2})$, $(P_{4,1}, Z_{4,1})$ and $(P_{4,2}, Z_{4,2})$. Output: original image S , secret information I .

Step 1. Use W_4 and Eq. 3.10 to generate predictive errors in the reverse order of the hiding phase. Use $(P_{4,1}, Z_{4,1})$, $(P_{4,2}, Z_{4,2})$ and Eq. 3.14 to extract information I_4 , and use Eq. 3.15 to recover the prediction errors. Let $I_{4,n}$ denote the n -th bit in I_4 .

$$I_{4,n} = \begin{cases} 0, & \text{if } D_{i,j} = P_{4,1} \text{ or } D_{i,j} = P_{4,2}; \\ 1, & \text{if } D_{i,j} = P_{4,1} - 1 \text{ or } D_{i,j} = P_{4,2} + 1. \end{cases} \quad (3.14)$$

$$D'_{i,j} = \begin{cases} D(i,j) + 1, & Z_{4,1} < D_{i,j} \leq P_{4,1} - 1; \\ D_{i,j} - 1, & P_{4,2} + 1 \leq D_{i,j} < Z_{4,2}. \end{cases} \quad (3.15)$$

Step 2. Use Eq. 3.13 to reconstruct the pixel values for the fourth stage.

Step 3. For all the remaining stages, repeat steps 1-3 to extract the inserted secret information I_3, I_2 and I_1 and reconstruct the corresponding pixels.

Step 4. Output original image S and secret information $I = I_1 || I_2 || I_3 || I_4$.

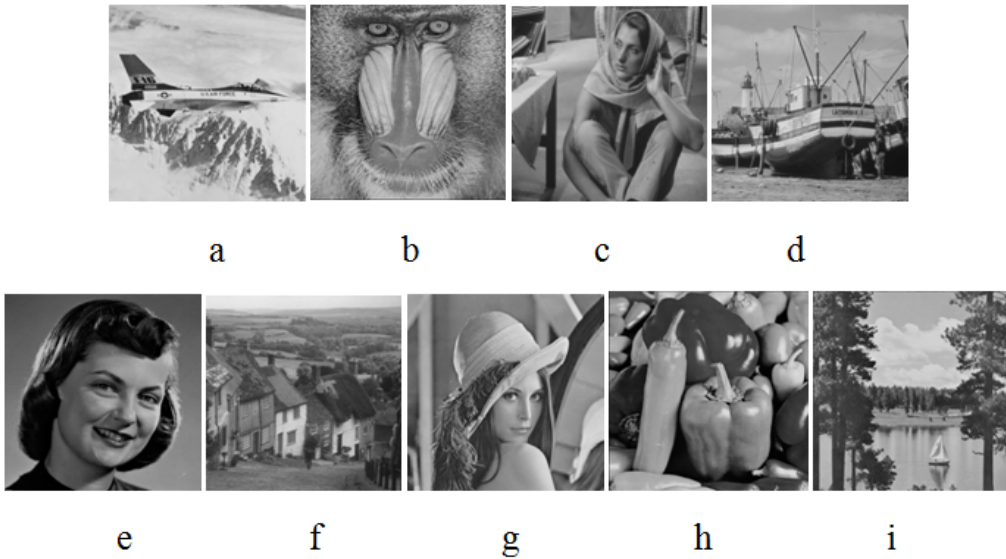


FIGURE 4. Test images - (a)Airplane, (b)Baboon, (c)Barbara, (d)Boat, (e)Girl, (f)Goldhill, (g)Lena, (h)Peppers, (i)Sailboat

4. Experimental results. In this section, we demonstrate the effectiveness of our proposed method by comparing with the three methods by Hong *et al.* [13], Yang *et al.* [2] and Lin *et al.* [18]. We use nine well-known 512×512 grayscale images as the cover images Airplane, Baboon, Barbara, Boat, Girl, Goldhill, Lena, Peppers and Sailboat, as shown in Fig. 4. To illustrate the effect of image size on the weighted prediction scheme, we consider five cases - 32×32 , 64×64 , 128×128 , 256×256 and 512×512 . The experimental results for these methods are displayed in Table 1 to Table 5.

The results in these tables can be summarized as follows: (1) the PSNR's by the 3-by-3 grid and weighted prediction methods are similar to or better than those by the chess board and Hong's methods; (2) in terms of the payload, the 3-by-3 grid and weighted prediction methods generally outperform the other two methods. In order to further compare the difference among these methods, Figs. 5(a)-(i) display the corresponding payloads for the images of various sizes of $2^n \times 2^n$.

TABLE 1. Results of 32×32 images

32 × 32								
	Hong		Chess Board		3-by-3 Grid		Weight	
	Payload (bpp)	PSNR (dB)						
Airplane	0.10	48.64	0.11	51.87	0.12	51.94	0.13	52.18
Baboon	0.06	48.54	0.11	49.72	0.11	50.03	0.15	49.60
Barbara	0.08	48.57	0.08	49.93	0.08	51.02	0.14	50.58
Boat	0.13	48.70	0.13	50.64	0.12	51.61	0.21	50.30
Girl	0.14	48.73	0.17	50.74	0.17	51.31	0.19	50.89
Goldhill	0.10	48.65	0.09	50.37	0.09	49.97	0.17	50.03
Lena	0.11	48.67	0.10	50.25	0.10	51.58	0.18	50.30
Peppers	0.08	48.59	0.09	50.64	0.08	52.11	0.14	50.15
Sailboat	0.06	48.54	0.06	51.90	0.06	52.71	0.08	52.88
Average	0.10	48.62	0.10	50.67	0.10	51.36	0.15	50.77

TABLE 2. Results of 64×64 images

64 × 64								
	Hong		Chess Board		3-by-3 Grid		Weight	
	Payload (bpp)	PSNR (dB)						
Airplane	0.12	48.55	0.14	49.45	0.18	49.80	0.20	49.73
Baboon	0.07	48.44	0.09	48.90	0.11	48.89	0.13	49.06
Barbara	0.14	48.60	0.14	48.92	0.15	48.95	0.26	49.29
Boat	0.18	48.72	0.22	49.14	0.23	49.34	0.28	49.35
Girl	0.21	48.79	0.28	49.40	0.32	49.63	0.35	49.59
Goldhill	0.13	48.58	0.12	48.77	0.15	48.96	0.22	49.11
Lena	0.17	48.70	0.19	49.10	0.22	49.25	0.32	49.57
Peppers	0.15	48.64	0.17	49.21	0.18	49.22	0.27	49.37
Sailboat	0.09	48.49	0.09	49.07	0.10	49.31	0.12	49.26
Average	0.14	48.61	0.16	49.11	0.18	49.26	0.24	49.37

TABLE 3. Results of 128×128 images

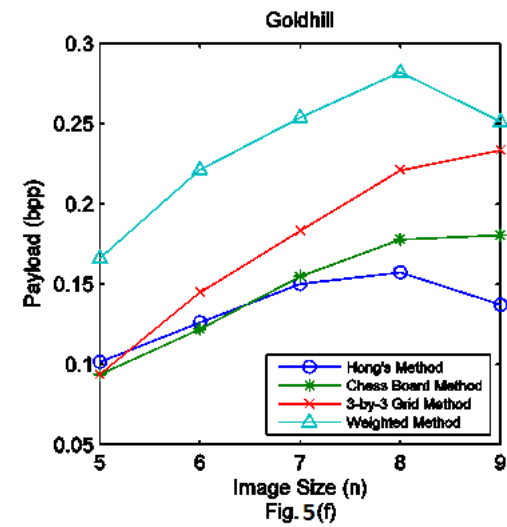
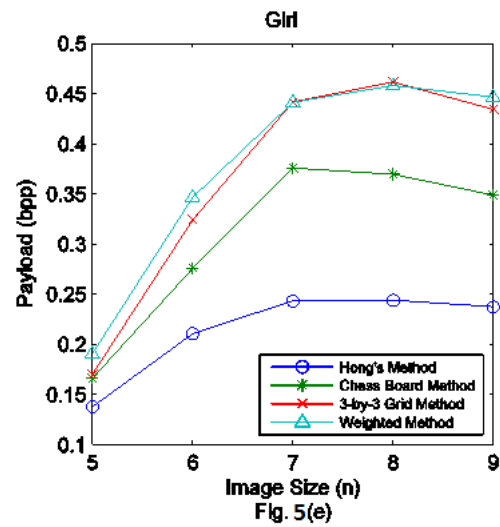
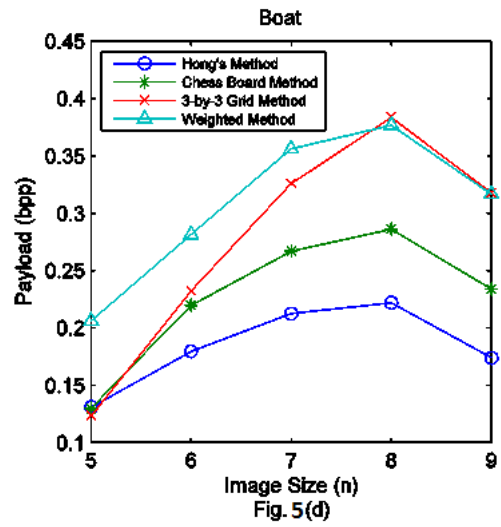
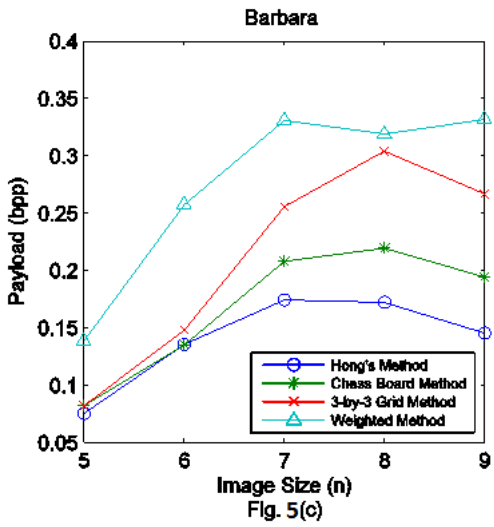
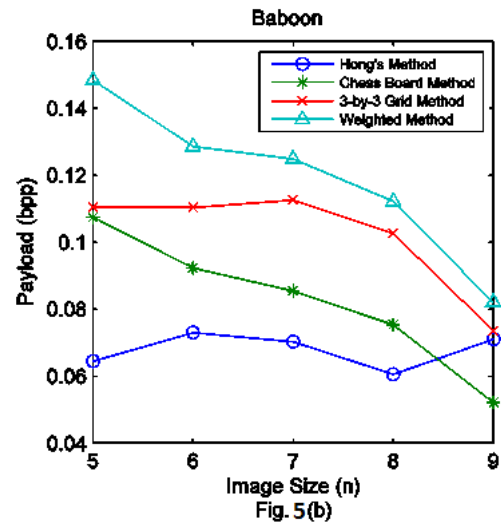
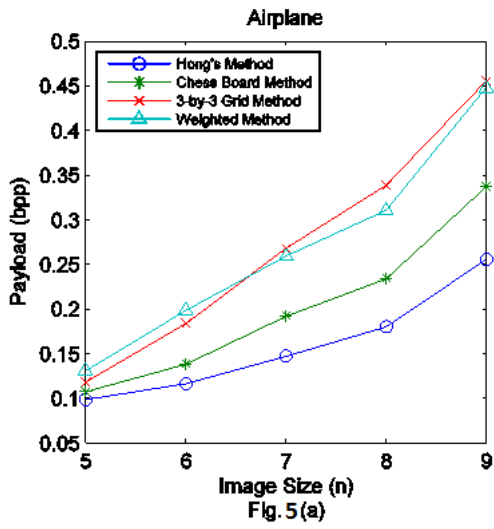
128 × 128								
	Hong		Chess Board		3-by-3 Grid		Weight	
	Payload (bpp)	PSNR (dB)						
Airplane	0.15	48.54	0.19	48.79	0.27	49.00	0.26	48.98
Baboon	0.07	48.37	0.09	48.64	0.11	48.63	0.12	48.67
Barbara	0.17	48.60	0.21	48.77	0.26	48.90	0.33	49.09
Boat	0.21	48.69	0.27	48.95	0.33	49.10	0.36	49.21
Girl	0.24	48.76	0.38	49.26	0.44	49.49	0.44	49.47
Goldhill	0.15	48.54	0.15	48.64	0.18	48.73	0.25	48.89
Lena	0.20	48.65	0.26	48.91	0.33	49.10	0.41	49.34
Peppers	0.19	48.63	0.25	48.87	0.31	49.05	0.36	49.23
Sailboat	0.07	48.38	0.10	48.66	0.15	48.67	0.14	48.72
Average	0.16	48.57	0.21	48.83	0.26	48.96	0.30	49.07

TABLE 4. Results of 256×256 images

256 × 256								
	Hong		Chess Board		3-by-3 Grid		Weight	
	Payload (bpp)	PSNR (dB)						
Airplane	0.18	48.58	0.23	48.76	0.34	49.04	0.31	48.96
Baboon	0.06	48.30	0.08	48.35	0.10	48.47	0.11	48.54
Barbara	0.17	48.56	0.22	48.71	0.30	48.93	0.32	48.99
Boat	0.22	48.68	0.29	48.88	0.38	49.15	0.38	49.13
Girl	0.24	48.73	0.37	49.11	0.46	49.43	0.46	49.41
Goldhill	0.16	48.52	0.18	48.61	0.22	48.72	0.28	48.87
Lena	0.21	48.64	0.28	48.86	0.38	49.15	0.41	49.22
Peppers	0.20	48.62	0.28	48.87	0.37	49.10	0.36	49.08
Sailboat	0.12	48.43	0.15	48.56	0.21	48.69	0.22	48.73
Average	0.17	48.56	0.23	48.75	0.31	48.97	0.32	48.99

TABLE 5. Results of 512×512 images

512 × 512								
	Hong		Chess Board		3-by-3 Grid		Weight	
	Payload (bpp)	PSNR (dB)						
Airplane	0.26	48.74	0.34	48.97	0.46	49.30	0.45	49.27
Baboon	0.07	48.30	0.05	48.36	0.07	48.32	0.08	48.35
Barbara	0.15	48.47	0.19	48.61	0.27	48.79	0.33	48.96
Boat	0.17	48.54	0.23	48.71	0.32	48.92	0.32	48.92
Girl	0.24	48.70	0.35	49.00	0.43	49.31	0.45	49.34
Goldhill	0.14	48.46	0.18	48.58	0.23	48.71	0.25	48.75
Lena	0.18	48.55	0.25	48.75	0.34	48.98	0.34	48.99
Peppers	0.13	48.43	0.18	48.58	0.29	48.84	0.27	48.79
Sailboat	0.11	48.40	0.16	48.52	0.26	48.77	0.22	48.68
Average	0.16	48.51	0.21	48.67	0.30	48.88	0.30	48.89



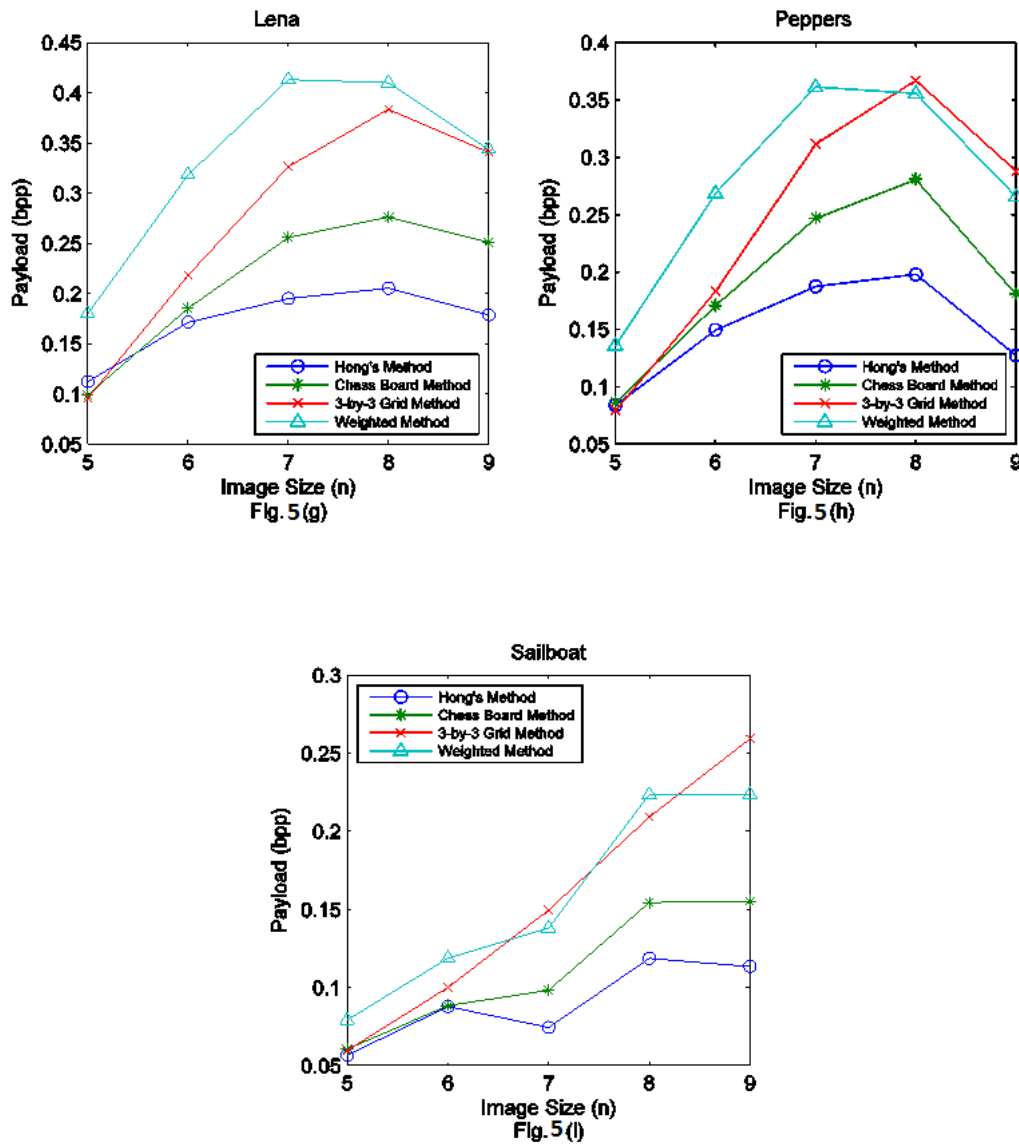


FIGURE 5. Relationship of payload and image size

As can be seen again, the 3-by-3 grid and weighted prediction methods generally outperform the other two methods over the night images and various image sizes. It is also noticeable that, for most of the image sizes with $n \leq 8$, the performance of the weighted prediction method is either similar to or better than that of the 3-by-3 grid method. To further understand the difference between the 3-by-3 grid and weight-based methods, Figs. 6(a)-(d) provide an illustration on the histograms of the differences of adjacent pixels for Girl, Airplane, Goldhill and Baboon of $2^7 \times 2^7$ pixels (i.e., $n = 7$ in Fig. 5). Typically the smoother the images, the more centralized the differences of adjacent pixels [23]. As such, we can consider Girl and Airplane as smooth images, and Goldhill and Baboon as complex ones. For these images, Figs. 5(e) and (a) show the payloads by the 3-by-3 grid and weighted prediction methods for Girl and Airplane are similar, respectively. However, for complex images Goldhill and Baboon, Figs. 5(f) and (b) show that our proposed weighted prediction method obviously outperform the 3-by-3 grid prediction method. For the same reason, over most of the image sizes, Babara, Boat, Lena, and Peppers can be

regarded as complex images, and the weighted prediction method thus outperforms the 3-by-3 grid method, as well.

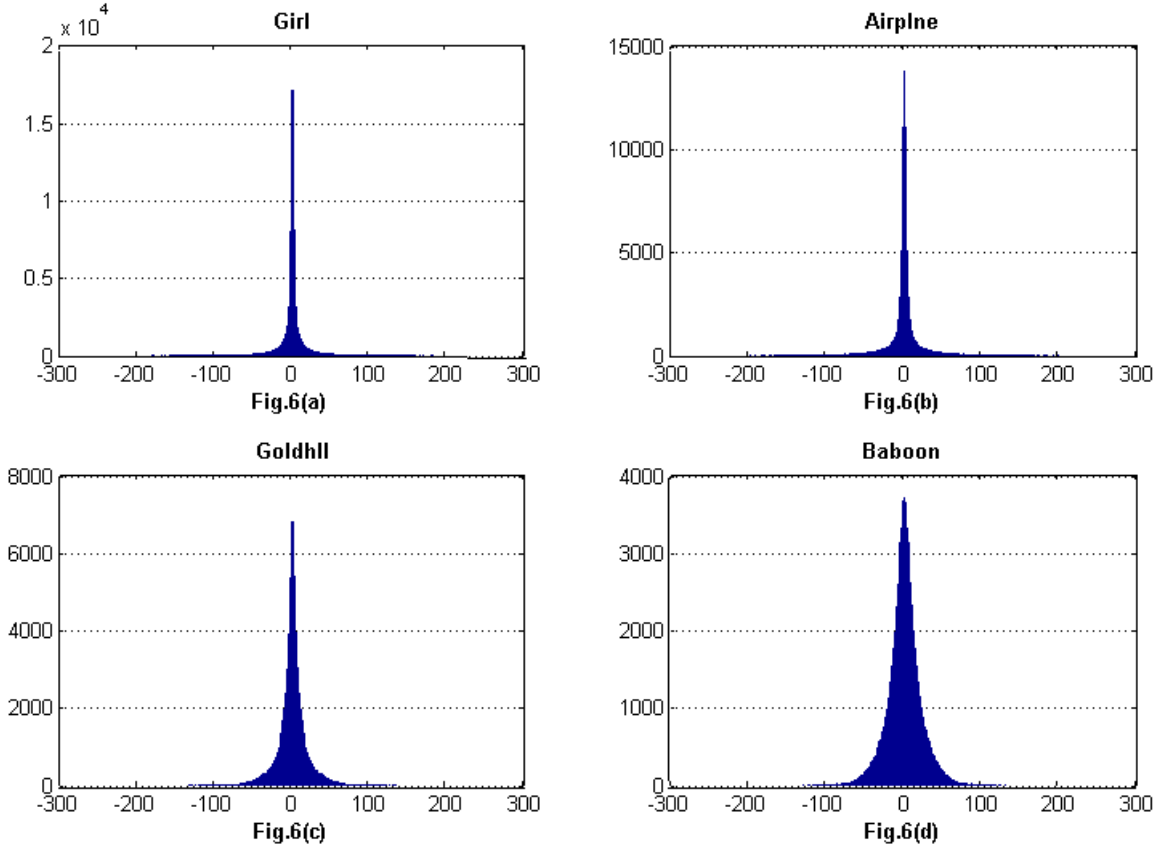


FIGURE 6. Histogram of images by our proposed method

In addition, as Theorem 1 in Section 3 points out, the least-square error increases as the size of the image increases, which may in turn impede the performance of our optimal weight-based prediction method. We thus notice that the results for large n (e.g., $n = 9$) in complex images such as Goldhill and Lena, the payload performance of the optimal eight-based method over the 3-by-3 grid method degrades. However, for the even more complex image Baboon, our method can still outperform the 3-by-3 grid method for large n . To sum up, the weighted prediction method is a superior data-hiding scheme over the 3-by-3 grid method, and is certainly a much better option over the other two popular methods.

5. Conclusions. In this paper, we present a novel weight-based prediction method to improve several existing reversible data hiding methods. Using the solution of the least-squares problem, we obtain the optimal set of weights for the neighboring pixels to improve the prediction accuracy of the target and thus increase the payload capacity.

The effectiveness of this approach has been demonstrated using several well-known test images. The empirical results showed that our proposed method significantly improves the embedding capacity over these existing methods and still maintains the quality of stego-images.

REFERENCES

- [1] X. Gao, L. An, X. Li, and D. Tao, Reversibility improved lossless data hiding, *Journal of Signal Processing*, vol. 89, pp. 2053-2065, 2009.
- [2] C. H. Yang, and M. H. Tsai, Improving histogram-based reversible data hiding by interleaving predictions, *IET Image Processing*, vol. 4, pp. 223-234, 2010.
- [3] J. Y. Hsiao, K. F. Chan, and J. M. Chang, Block-based reversible data embedding, *Journal of Signal Process*, vol. 89, no. 4, pp. 556-569, 2009.
- [4] D. M. Thodi, and J. J. Rodriguez, Expansion embedding techniques for reversible watermarking, *IEEE Trans. Image Processing*, vol. 16, no. 3, pp. 723-730, 2007.
- [5] H. J. Kim, V. Sachnev, Y. Q. Shi, J. Nam, and H. G. Choo, A novel difference expansion transform for reversible data embedding, *IEEE Trans. Information Forensics and Security*, vol. 3, no. 3, pp. 456-465, 2008.
- [6] J. H. Lin, F. Masaaki, and K. Hitoshi, Lossless data hiding in the spatial domain for high quality image, *IEICE Transa. Fundamentals of Electronics*, vol. E90-A, no. 4, pp. 771-777, 2007.
- [7] J. Tian, Reversible data embedding using a difference expansion, *IEEE Trans. Circuits and Systems for Video Technology*, vol. 13, no. 8, pp. 890-896, 2003.
- [8] C. C. Chang, and T. C. Lu, A difference expansion oriented data hiding scheme for restoring the original host images, *Journal of Systems and Software*, vol. 79, no. 12, pp. 1754-1766, 2006.
- [9] A. M. Alattar, Reversible watermark using the difference expansion of generalized integer transform, *IEEE Trans. Image Processing*, vol. 13, no. 8, pp. 1147-1156, 2004.
- [10] H. W. Tseng, and C. P. Hsien, Prediction-based reversible data hiding, *Journal of Information Sciences*, vol. 179, pp. 2460-2469, 2009.
- [11] C. C. Chang, C. C. Lin, C. S. Tseng, and W. L. Tai, Reversible hiding in DCT-based compressed images, *Journal of Information Sciences*, vol. 177, no. 13, pp. 2768-2786, 2007.
- [12] Z. Ni, Y. Q. Shi, N. Ansari, and W. Su, Reversible data hiding, *IEEE Trans. Circuits and Systems for Video Technology*, vol. 16, pp. 354-362, 2006.
- [13] W. Hong, T. S. Chen, and C. W. Shiu, Reversible data hiding for high quality images using modification of predictive errors, *The Journal of Systems and Software*, vol. 82, no. 11, pp. 1833-1842, 2009.
- [14] P. Tsai, Y. C. Hu, and H. L. Yeh, Reversible image hiding scheme using predictive coding and histogram shifting, *Journal of Signal Processing*, vol. 89, pp. 1129-1143, 2009.
- [15] C. C. Lin, and N. L. Hsueh, A lossless data hiding scheme based on three-pixel block differences, *Journal of Pattern Recognition*, vol. 41, no. 4, pp. 1415-1425, 2008.
- [16] C. C. Lin, W. L. Tai, and C. C. Chang, Multilevel reversible data hiding based on histogram modification of difference images, *Journal of Pattern Recognition*, vol. 41, no. 12, pp. 3582-3591, 2008.
- [17] E. Chrysochos, V. Fotopoulos, A. N. Skodras, and M. Xenos, Reversible image watermarking based on histogram modification, *Proc. of the 11th Panhellenic Conference on Informatics with international participation*, vol. B, pp. 93-104, 2007.
- [18] S. L. Lin, Y. T. Cheng, C. Y. Chen, and N. Y. Shih, A reversible information hiding method by a histogram-based 3×3 box filter, *Proc. of Taiwan Academic Network Conference*, pp. B94-B100, 2009.
- [19] R. C. Gonzalez, and R. E. Woods, *Digital Image Processing*, 3rd Ed., Prentice Hall, 2008.
- [20] M. J. Weinberger, G. Seroussi, and G. Sapiro, The LOCO-I lossless image compression algorithm: principles and standardization into JPEG-LS, *IEEE Trans. Image Processing*, vol. 9, no. 8, pp. 1309-1324, 2000.
- [21] D. Salomon, *Data Compression: The Complete Reference*, 2nd Ed., Springer, 2000.
- [22] J. L. Steven, *Linear Algebra with Applications*, 7th Ed., Pearson Education Limited, 2006.
- [23] Z. Li, X. P. Chen, X. Z. Pan and Z. T. Zeng, Lossless Data Hiding Scheme Based on Adjacent Pixel Difference, *Proc. of International Conference on Computer Engineering and Technology*, vol. 1, pp. 588-592, 2009.